Published in final edited form as:

J Immunol. 2016 October 15; 197(8): 3214–3224. doi:10.4049/jimmunol.1600663.

Circulating Memory CD4+ T Cells Target Conserved Epitopes of Rhinovirus Capsid Proteins and Respond Rapidly to Experimental Infection in Humans

Lyndsey M. Muehling, MS[†,*], **Duy T. Mai, MS**[‡,*], **William W. Kwok, PhD**, **Peter W. Heymann, MD**[¶], **Anna Pomés, PhD**[‖], and **Judith A. Woodfolk, MBChB, PhD**[†]

[†]Department of Medicine, University of Virginia Health System, Charlottesville, VA

[‡]Benaroya Research Institute at Virginia Mason, Seattle, WA

[¶]Department of Pediatrics, University of Virginia Health System, Charlottesville, VA

[‖]Indoor Biotechnologies Inc., Charlottesville, VA

Abstract

Rhinovirus (RV) is a major cause of common cold and an important trigger of acute episodes of chronic lung diseases. Antigenic variation across the numerous RV strains results in frequent infections and a lack of durable cross-protection. Since the nature of human CD4$^+$ T cells that target RV is largely unknown, T-cell epitopes of RV capsid proteins were analyzed, and cognate T cells characterized in healthy subjects and those infected by intranasal challenge. Peptide epitopes of the RV-A16 capsid proteins VP1 and VP2 were identified by peptide/MHCII tetramer-guided epitope mapping (TGEM), validated by direct *ex vivo* enumeration, and interrogated using a variety of *in silico* methods. Among non-infected subjects, those circulating RV-A16-specific CD4$^+$ T cells detected at the highest frequencies targeted 10 unique epitopes that bound to diverse HLA-DR molecules. T-cell epitopes localized to conserved molecular regions of biological significance to the virus, were enriched for HLA class I and II binding motifs, and constituted both species-specific (RV-A) and pan-species (RV-A, -B and -C) varieties. Circulating epitope-specific T cells comprised both memory Th1 and T follicular helper cells, and were rapidly expanded and activated after intranasal challenge with RV-A16. Cross-reactivity was evidenced by identification of a common *0401-restricted epitope for RV-A16 and RV-A39 by TGEM, and the ability for RV-A16-specific Th1 cells to proliferate in response to their RV-A39 peptide counterpart. The preferential persistence of high-frequency RV-specific memory Th1 cells that recognize a limited set of conserved epitopes likely arises from iterative priming by previous exposures to different RV strains.

Keywords

Human; viral; T cells; antigens/peptides; epitopes

Corresponding author: Judith A. Woodfolk, MBChB, PhD, Allergy Division, PO Box 801355, University of Virginia Health System, Charlottesville, VA 22908-1355. Tel: 434-924-1293; Fax: 434-924-5779; jaw4m@virginia.edu.

*L. Muehling and D. Mai contributed equally to this manuscript.

Introduction

Infection with human rhinovirus (RV) accounts for over half of all cases of common cold, and usually runs a benign course. However, among those with chronic respiratory disorders, RV infection induces disease exacerbations that often require hospitalization and, in the worst cases, can be fatal (1–6). Rhinovirus is especially problematic for children suffering from allergic asthma, not only because of its link to acute wheezing episodes, but its purported contribution to asthma pathogenesis in early life (7–9). Repeat infections are common, with children experiencing a particularly high annual incidence of 6 to 8 colds (10). Although elderly people experience fewer infections than children, the burden of disease presented by RV is greater than that of other respiratory viruses commonly associated with complications, and is especially problematic for adults with chronic obstructive pulmonary disease (11). Together, these factors create an enormous economic and public health burden.

Human rhinovirus is a single-stranded RNA virus of the Picornaviridae family. Infection results in the production of serotype-specific serum neutralizing antibodies that confer protection from re-infection with the same strain, and reduce symptom severity upon experimental challenge with the same serotype (12–15). However, antibody responses are transient, and cross-neutralization among the numerous RV types is limited, owing to their high degree of antigenic variability (16–18).

There is mounting evidence to support a protective role for $CD4^+$ T cells in response to a variety of respiratory viruses, including RV (19–22). Among seronegative subjects who were experimentally infected with RV, higher *in vitro* T-cell proliferation and IFN-γ production in response to RV before infection was linked to reduced viral shedding (22). Despite the numerous reports of T-cell epitopes within capsid proteins of diverse viruses, no studies have explored RV. The RV capsid comprises four proteins (designated VP1 through 4) that assemble to form an icosahedral structure containing the determinants necessary for cell entry (23–26). Exposure of VP1 and VP2 on the capsid surface makes them attractive targets for an immune response. This is evidenced by the ability to readily detect anti-VP1 antibodies, including IgG, in serum (27–30). In a mouse model, immunization with conserved capsid proteins of RV-A16 induced cross-reactive immune responses driven by $CD4^+$ T cells, which were associated with more rapid viral clearance (31). These fundamental studies suggest that capsid proteins warrant further evaluation as T-cell targets in humans.

We hypothesized that circulating memory $CD4^+$ T cells capable of recognizing different RV strains would be readily detected in adults, owing to repeated priming by previous RV infections. Here, we describe the development of MHCII tetramers displaying peptide epitopes of the clinically relevant strain RV-A16, to characterize circulating $CD4^+$ T cells specific for VP1 and VP2 (11, 29, 32–37). By integrating *in vitro* and *in silico* epitope mapping, we validate and interrogate immunodominant epitopes recognized by circulating $CD4^+$ T cells in healthy subjects, and establish their cross-reactive potential. Rapid expansion and activation of epitope-specific memory T cells in an experimental infection

model following intranasal challenge with RV-A16, supports a central role for cross-reactive $CD4^+$ T cells in adaptive immunity to RV.

Methods

Human Subjects

Studies were carried out in 61 healthy adults (ages 18–45). All subjects were asymptomatic and reported no cold symptoms in the previous 4 days. Written informed consent was obtained from all participants and studies were approved by the University of Virginia Human Investigation Committee and the Institutional Review Board of Benaroya Research Institute. In addition, rhinovirus challenge studies were approved by the FDA and the NIAID Safety Committee (Clinical Trials.gov ID NCT02111772).

Intranasal Challenge with RV-A16

Four non-allergic subjects (total IgE <30 IU/ml) who lacked serum neutralizing antibodies for RV-A16 were challenged with 1 ml of inoculum containing 300 $TCID_{50}$ of live RV-A16 (0.5 ml per nostril) (38). Infection was confirmed based on ≥4-fold rise in serum neutralizing titer at 3 weeks post-inoculation and/or positive qPCR for RV-A16 in nasal washes (39). Upper respiratory tract symptoms were assessed using a modification of the Jackson criteria (40).

PBMC Isolation and HLA Typing

PBMCs were isolated from heparinized venous blood by Ficoll gradient centrifugation (41, 42). DNA samples were HLA-typed using DRB1 SSP Unitray Kits (Invitrogen, Carlsbad, California) according to the manufacturer's instructions.

Flow Cytometry Antibodies and Reagents

Fluorochrome-conjugated monoclonal antibodies for flow cytometry were as follows: anti-CD3 (clone SK7), anti-CD4 (L200), anti-CD14 (MϕP9), anti-CD19 (SJ25C1), anti-CD45RA (HI100), anti-CD185 (RF8B2), anti-CD279 (EH12.1), anti-IL-4 (8D4-8) (BD Biosciences, San Jose, CA, USA); anti-CD4 (clone SK3), anti-CD25 (BC96), anti-CD45RO (UCHL1), anti-CD127 (A019D5), anti-CD183 (G025H7), anti-CD185 (J252D4), anti-CD197 (G043H7), anti-IFN-γ (B27), anti-IL-17A (BL168), anti-IL-21 (3A3-N2) (Biolegend, San Diego, CA, USA); anti-CD194 (clone 205410) (R&D Systems, Minneapolis, MN, USA); anti-CD3 (clone UCTH1), anti-CD4 (OKT4), anti-CD14 (61D3), anti-CD19 (SJ25C1), anti-CD25 (BC96) (eBioscience, San Diego, CA, USA). Compensation beads were obtained from BD Biosciences, and aqua viability dye was obtained from Invitrogen (Carlsbad, CA, USA). Fix & Perm solution and Alexa Fluor® 568 Protein Labeling Kits were obtained from Life Technologies (Carlsbad, CA, USA). A custom RV-A39 peptide ($VP2_{169\text{-}188}$: SDDNWLNFDGTLLGNLLIFP, >90% purity) was obtained from New England Peptides (Gardner, MA, USA).

Tetramer Guided Epitope Mapping and Surface Phenotyping of Tetramer-Positive Cells

Peptide libraries consisting of 20mers with a 12 amino acid overlap were generated to span the VP1, VP2 and VP4 protein sequences of RV-A16, and the VP1 and VP2 protein sequences of RV-A39 (UniprotKB accession #Q82122, Q5XLP5, http://www.uniprot.org/) (43). Peptide/MHC class II (pMHCII) tetramers for different HLA-DR molecules (DRB1*0101, *0301, *0401, *0404, *0701, *1101, *1501, and DRB5*0101) were then assembled, and displayed either pooled or individual peptides (44). Biologically relevant pMHCII complexes were identified by tetramer-guided epitope mapping (TGEM) using 2 steps: (1) PBMC cultures established from subjects with known HLA-DR types were stimulated with RV peptide pools derived from VP1, VP2, or VP4, and then stained with pMHCII tetramer pools; (2) positive signals were de-convoluted by repeating and staining with single-peptide tetramers. Tetramers that gave strong positive signals (~1% of total $CD4^+$ T cells) in the single peptide-tetramer screen in multiple subjects were then re-tested for their ability to detect RV-specific $CD4^+$ T cells in non-stimulated PBMCs (denoted as *ex vivo* analysis) in multiple subjects. In order to detect RV-specific T cells directly *ex vivo*, $tetramer^+$ cells were enriched by passing tetramer-stained PBMCs over an anti-PE magnetic column (Miltenyi Biotec, Auburn, CA, USA). Precursor frequencies of circulating $tetramer^+$ cells were then calculated by established methods (45). All experiments were performed in subjects expressing HLA-DR molecules corresponding to the selected tetramer. $Tetramer^+$ cells were phenotyped for surface markers by staining PBMCs with PE-conjugated tetramers, labeling with anti-PE magenetic beads, enriching with an AutoMACS separator (Miltenyi Biotec, Auburn, CA, USA), and then counterstaining for surface markers. A tetramer displaying an irrelevant peptide, the diabetes-associated antigen glutamic acid decarboxylase (GAD) 67 epitope (GAD555-567), was used as a negative control (46). For simplicity, identified RV-A16 peptide epitopes were given a numerical designation.

Assay To Assess T-Cell Cross-Reactivity

RV-specific $CD4^+$ T cells were expanded *in vitro* using established methods (44). Briefly, PBMCs from HLA-DRB1*0401+ subjects were stimulated with RV-A39 $VP2_{169\text{-}188}$, or else left unstimulated, for 14 days. Supplemental IL-2 (10 U/ml) was added on day 7. Cells were then stained with pMHCII tetramers and re-stimulated with PMA and ionomycin in the presence of Brefeldin A before staining for intracellular cytokines (47). Cells were analyzed on a BD LSR Fortessa (UVA Flow Cytometry Core Facility), and data analysis was performed using FlowJo version 9.3.3 (Tree Star Inc., Ashland, OR). Analysis of cytokine signatures was performed using SPICE version 5.3, downloaded from http://exon.niaid.nih.gov (48).

Sequence Alignment Algorithms

Amino acid sequences of RV-A16 epitopes were compared with other RV strains by protein BLAST search (NCBI) (49). Multiple sequence alignments were analyzed using Jalview v. 2.8.2 (50).

HLA Binding and Epitope Prediction

MHCII binding predictions for RV-A16 and RV-A39 polyproteins were generated using the Immune Epitope Database (IEDB) Consensus method (51, 52). This method integrates 3 different epitope prediction methods—SMM-align, NN-align, and the combinatorial peptide scanning library (Comblib)—in order to identify a 15mer consensus epitope (51–54). In cases where Comblib was not available for a given allele, the Sturniolo method was used (55). MULTIPRED2, an epitope prediction program that utilizes the NetMHCpan and NetMHCIIpan algorithms, was used to predict 9mer core epitopes for numerous alleles corresponding to HLA supertypes (56–59). This analysis was performed for the major HLA class II DR supertypes containing alleles used in TGEM (DR1, DR3, DR4, DR7, DR11 and DR15), as well as minor class II DR supertypes and class I supertypes. NetMHCIIpan was used to predict 19mer class II epitopes for single HLA alleles.

Location of T-Cell Epitopes in the Three-Dimensional Structure of the RV-A16 Capsid

The location of T cell epitopes within the three-dimensional structure of RV-A16 capsid proteins and the creation of structural images were performed with PyMol, based on the X-ray crystal structure of native RV-A16 at 2.15 Å resolution (PDB code 1aym) (60, 61).

Statistical Analysis

Percentages of $CD4^+$ T cells with discrete phenotypes were compared by the Wilcoxon matched-pairs signed rank test for paired analyses, and the Mann-Whitney test for unpaired analyses. Linear mixed models with Bonferroni correction were used to analyze longitudinal data (62).

Results

RV-A16 Epitopes Bind Multiple HLA Molecules and are Conserved

We first sought to identify RV-specific $CD4^+$ T cells in the blood of healthy subjects, and to interrogate their epitope specificity by TGEM (44). Two external capsid proteins (VP1 and VP2) and one internal capsid protein (VP4) of RV-A16 were selected for analysis. TGEM was performed in 24 subjects in the context of eight common HLA-DR molecules that provide ≥80% coverage of the US population. This process, which involved *in vitro* stimulation of PBMC cultures with RV peptides, yielded 45 pMHCII tetramers displaying 30 candidate epitopes of VP1 and VP2 (Supplemental Table I). No epitopes of VP4 were identified. Twelve tetramers provided reliable signals when used for direct *ex vivo* staining of PBMCs (≥2 $tetramer^+$ cells per million $CD4^+$ T cells in ≥3 subjects, n=29), yielding frequencies of up to 247 per million $CD4^+$ T cells (Figs. 1A–C, Supplemental Fig. 1). Four of these validated tetramers displayed VP1 epitopes and 8 displayed VP2 epitopes, corresponding to 3 and 7 unique epitopes, respectively (Figs. 1A & D). Two of these epitopes ($VP1_{P23}$ and $VP2_{P21}$), bound 2 different molecules each, indicating HLA promiscuity.

All epitopes mapped to regions of VP1 and VP2 that were highly conserved across 77 strains belonging to RV species A. Specifically, 8 of the 10 epitopes showed ≥85% amino acid sequence identity with >88% of all RV-A strains (Table I), including 3 that were

identical to >50% of all species A strains (63). Though the sequence identity was lower with RV-B strains, 6 epitopes had 65% to 95% sequence identity across ≥72% of RV-B strains. As expected, RV-A16 epitopes had the lowest identity with species C strains, which diverge in sequence from RV-A and RV-B species. Nonetheless, sequence similarities of ≥65% were observed for 7 of the epitopes. Together, these results confirm that circulating epitope-specific $CD4^+$ T cells detected at the highest frequencies in HLA-diverse subjects recognize conserved epitopes of external capsid proteins, including both species-specific and pan-species varieties.

HLA Class I and II Binding "Hotspots" Localize to Conserved Regions of VP1 and VP2

There was good agreement for $CD4^+$ T-cell epitopes identified by TGEM and those predicted by *in silico* methods. At least one consensus 15mer epitope containing a 9mer core epitope was predicted for each TGEM epitope in the context of its relevant HLA molecule using the IEDB consensus method (Fig. 1A). This algorithm accounts for the contribution of flanking residues to HLA binding (51–55). Furthermore, 11 of the 12 predicted consensus epitopes had a percentile rank in the top 10% of results, indicating strong predicted binding. Predicted 9mer core epitopes localized to molecular regions that were conserved across RV-A strains (Supplemental Fig. 2A). Core epitopes of $VP1_{P23}$ and $VP2_{P10}$ were the most highly conserved within the picornavirus family (Supplemental Fig. 2B).

To assess the contribution of peptide length to $CD4^+$ T-cell epitopes, we used an algorithm that predicts 9mer core epitopes for HLA supertypes encompassing 1,077 class I and class II molecules, without accounting for the contributions of flanking residues (MULTIPRED2) (56). By this method, only two 9mer $CD4^+$ T-cell epitopes corresponding to any TGEM epitope were identified. These epitopes were nested within $VP1_{P23}$ (aa187-195) and $VP2_{P24}$ (aa189-197), and were predicted to bind those HLA molecules displaying the corresponding TGEM epitopes (ie. *0101 and *0701 for $VP1_{P23}$, and *0101 for $VP2_{P24}$), as well as >80% of molecules of the corresponding HLA supertype (Figs. 1A, 2A). No 9mer epitopes for VP4 were predicted by this method (data not shown). By contrast, 10 of the 12 epitopes identified by TGEM were predicted using a 19mer input for the same algorithm (Fig. 1A).

Since $CD8^+$ T cells are central to anti-viral responses, we queried whether RV-A16 epitopes might provide a target for $CD8^+$ T cells. Using MULTIPRED2, a high density of class I binding motifs was predicted for HLA-A, -B, and -C supertypes spanning two regions, designated "A" (VP1 aa140-200) and "B" (VP2 aa160-220) (Fig. 2B). Regions A and B also contained multiple $CD4^+$ T-cell epitopes identified by TGEM and predicted binding motifs for common and less common HLA-DR supertypes (Fig. 2A). Motifs were predicted for molecules belonging to all HLA class I supertypes, including >55% of molecules within most HLA-A and HLA-B supertypes. Together, these results confirm the potential for conserved epitopes of RV-A16 to bind a broad array of HLA molecules, and to activate both $CD4^+$ and $CD8^+$ T cells.

VP1 Epitopes of RV-A16 Map to the Hydrophobic Binding Pocket

The existence of conserved T-cell epitopes of capsid proteins might seem to contradict the selective pressures that drive antigenic diversity of RV species. Thus, we explored whether

T-cell epitopes mapped to regions of functional significance for the virus. Analyses in the context of the oligomeric subunit formed by the capsid proteins VP1-4, revealed that all T-cell epitopes contained residues exposed on external and/or internal surfaces of the viral capsid (Figs. 3A & B). Additionally, most epitopes mapped to the interface of adjacent oligomeric subunits.

Most RV-A and RV-B strains gain entry into host cells via surface ICAM-1, whereas RV-C uses an alternate mode of entry (23–26). ICAM-1 binds in a canyon within VP1 containing a hydrophobic binding pocket, which is occupied by a pocket factor that regulates viral entry, uncoating and assembly (Fig. 3C). Positional analyses in the context of the three-dimensional structure of VP1-4 revealed that each VP1 epitope mapped to the hydrophobic binding pocket of RV-A16, with two residues of the $VP1_{P18}$ core epitope (Pro1146 and Tyr1144) residing close to the pocket factor (Fig. 3D) (61, 64).

Pre-existing Epitope-Specific Memory Th1 Cells Respond Rapidly to RV-A16 Infection

Repeated T cell priming by previous RV infections caused by different virus strains would be expected to induce circulating memory $CD4^+$ T cells that preferentially target conserved RV epitopes at higher numbers than those recognizing less well-conserved regions of capsid proteins. Consistent with this theory, direct *ex vivo* analysis of "untouched" $tetramer^+$ cells in healthy subjects revealed a predominant memory phenotype (>60% $CD45RA^{neg}$) displaying a Th1 signature ($CXCR3^+CCR4^{neg}$) that was uniform across all epitope specificities (Fig. 4A & B) (65–67). $Tetramer^+$ cells included a $CXCR5^+$ subset, suggesting the presence of T follicular helper (Tfh) cells with lymph node-homing capabilities.

Next, we tested the capacity for pre-existing epitope-specific memory Th1 cells to respond following *in vivo* exposure to RV. To do this, subjects who tested seronegative for RV-A16 were experimentally infected by intranasal inoculation with RV-A16. Immediately prior to inoculation, the presence of $tetramer^+$ T cells with a central memory phenotype ($CCR7^+CD45RO^+$) was confirmed in all subjects (Fig. 5A). Following inoculation with RV-A16, these subjects became infected and developed symptoms (Fig. 5B). Concomitant with infection, circulating epitope-specific memory $CD4^+$ T cells increased in numbers, and became activated based on reduced expression of IL-7Rα (Figs. 5C & D). These changes were evident within 4 days of virus inoculation, indicating rapid mobilization and activation of epitope-specific T cells. As expected, responding cells displayed a Th1 phenotype ($CXCR3^+CCR4^{neg}$) (Fig. 5E). These findings also established that conserved epitopes identified by TGEM are processed from intact virions and presented *in vivo* to pre-existing circulating memory Th1 cells.

Evidence of T-Cell Cross-Reactivity at the Epitope Level

Finally, we sought to identify cross-reactive T-cell epitopes between different RV strains. Tetramer guided epitope mapping of RV-A39, a group A virus that is serologically distinct from RV-A16, yielded 2 epitopes for DRB1*0401. One of these (designated $VP2_{169\text{-}188}$) contained a predicted core corresponding to that of the RV-A16 epitope, $VP2_{P21}$, and spanned a region with 100% sequence identity between RV strains (Fig. 6A). By contrast, no RV-A16 counterpart was identified for the other RV-A39 epitope. Stimulating cells from

HLA-DR*0401+ subjects with RV-A39 $VP2_{169\text{-}188}$ induced expansion of T cells specific for RV-A16 $VP2_{P21}$, despite different flanking residues (Figs. 6B & C). Expanded RV-specific T cells were predominantly IFN-γ^{+}IL-4^{neg}, consistent with a dominant Th1 subset. Minor populations expressing the Th17-associated cytokine IL-17A, and the Tfh-associated cytokine IL-21, were also identified (Figs. 6D & E). These findings establish proof-of-concept for cross-reactive $CD4^{+}$ T-cell determinants between different RV strains.

Discussion

By integrating *in vitro* and *in silico* epitope mapping approaches, we have constructed a comprehensive map of $CD4^{+}$ T-cell epitopes of the capsid proteins VP1 and VP2 of RV-A16. Our strategy allowed the identification of immunologically relevant epitopes in the context of multiple HLA molecules, and characterization of cognate $CD4^{+}$ T cells. We report that those circulating RV-specific memory $CD4^{+}$ T cells present at the highest frequencies in HLA-diverse subjects recognize a limited set of species-specific and pan-species epitopes. Our ability to readily identify circulating virus-specific memory T cells in healthy subjects supports the view that these T cells arise from repeated previous infections with homotypic or heterotypic RV strains, or related viruses.

Using an experimental infection model that capitalized on novel RV tetramers developed in this study, we were able to precisely track and enumerate epitope-specific memory T cells in subjects who were infected with RV-A16 *in vivo.* This approach demonstrated that pre-existing epitope-specific memory T cells responded rapidly to RV infection *in vivo* following intranasal challenge, thereby providing further evidence of T-cell priming by previous viral exposures. Pre-existing responding cells included Th1 effectors and Tfh cells, both of which would be expected to contribute to viral clearance through cytolysis, and by helping B cells produce antibodies (68–70). Importantly, observations in the RV challenge model provided proof-of-concept that those epitopes identified by TGEM were processed from intact virions and presented to T cells *in vivo* following infection with live virus, thereby supporting their immunological relevance.

Tetramer-guided epitope mapping provides a sensitive and comprehensive approach for identifying T-cell epitopes restricted to a specific HLA molecule (71–73). Our study design involved several analytical steps including identification of T-cell epitopes *in vitro* using peptide-stimulated cultures established from subjects with known HLA type, followed by validation by direct *ex vivo* staining of cells in additional subjects. The immunodominance of these epitopes was supported by the reliable detection of RV-specific $CD4^{+}$ T cells specific for each of the 10 validated epitopes in the context of 8 HLA-DR molecules, covering >80% of the general population. Indeed, RV-specific T cells targeting *the same* *0401-restricted epitope were readily detected in eleven *0401+ subjects included in our study. The ability for computer algorithms to predict those $CD4^{+}$ T-cell epitopes identified by TGEM further supported their significance. Moreover, enrichment of a broad array of class I HLA binding motifs within TGEM epitopes highlighted their potential to activate $CD8^{+}$ T cells in tandem with $CD4^{+}$ T cells.

A major advantage of our approach as compared with other epitope mapping methods, such as ELISPOT or intracellular cytokine assays, is that the epitopes identified by TGEM are proven to bind to specific MHC molecules. In addition, TGEM is highly sensitive based on its ability to detect frequencies as low as 1 in 300,000 $CD4^+$ T cells (71, 74). Assay sensitivity is critical given the low precursor frequency of antigen-specific T cells in the T-cell repertoire, and their random distribution in tissue culture wells. Thus, less sensitive methods often warrant the use of statistical modeling to confirm immunodominance (75).

The T-cell frequencies observed in our study were within the range of those reported using MHCII tetramers for other viral epitopes in the absence of current exposure, including those present several years after vaccination (72, 76). Since TGEM preferentially selects for T-cell epitope specificities that exist at the highest frequencies, our results imply selective persistence of T cells directed against conserved epitopes. This is consistent with iterative priming of specific memory T cells by epitopes common to multiple RV strains. In line with this theory, we provided proof-of-concept for shared T-cell epitopes among different RV strains. This observation was significant given that corresponding *0401-restricted epitopes were identified in separate TGEM experiments, using different peptide libraries spanning VP2 of RV-A16 and RV-A39. Our inability to identify a match from RV-A16 for a second *0401-restricted epitope of RV-A39 was likely explained by differences in sequence within the 9mer core epitope.

Positioning of T-cell epitopes within structural elements that interact with ICAM-1, and at protein interfaces that are likely involved in capsid protein assembly, might provide a structural basis for the conservation of RV epitopes. Interestingly, no T-cell epitopes of the small capsid protein VP4 were identified, and this was borne out by *in silico* analyses. VP4 is highly conserved across different RV strains, and is the only capsid protein that resides completely on the internal aspect of the capsid (77). While it would seem that VP4 should provide an attractive target for cross-reactive T cells based on its sequence conservation, its lack of MHCII binding motifs likely precludes MHC binding and induction of cognate T cells. Recent work has shown that VP4 separates from the capsid during viral cell entry to form multimeric pores within the host cell membrane that facilitate transmembrane transport of the viral genome (78). This aspect, which is presumably critical to viral pathogenesis, might explain its highly conserved nature. Regardless, failure to detect VP4 epitopes lends credence to the external capsid proteins, VP1 and VP2, as immunogenic antigens that promote durable $CD4^+$ T-cell responses.

It has been known for decades that serum neutralizing antibodies induced by RV infection protect against reinfection with the same strain (12–15). However, attempts to develop cross-protective antibody-based vaccines have been disappointing, owing to the high degree of antigenic variability among the numerous existing RV serotypes (18). By contrast, recent work in mice immunized with conserved capsid protein antigens has provided proof-of-concept for the capacity to induce cross-reactive immune responses driven by $CD4^+$ T cells (31). There are several lines of evidence to support a protective role for $CD4^+$ T cells in RV infection in humans. For example, RV-specific $CD4^+$ T-cell clones produce IFN-γ and proliferate in response to stimulation with multiple RV serotypes (79, 80). Moreover, higher proliferation and IFN-γ responses prior to RV infection have been linked to reduced viral

shedding after inoculation (22). In the present study, we identified a memory Th1 signature in circulating RV-specific T cells in healthy subjects, coupled with their rapid expansion following RV infection. Our ability to detect increases in circulating $CD4^+$ T cells recognizing a single epitope following intranasal challenge with RV was striking, given that infection is confined to the respiratory tract. Since levels of neutralizing antibodies typically peak 3–5 weeks post-inoculation (16), observations in our experimental infection model support a rapid anti-viral response mediated by pre-existing antigen-experienced $CD4^+$ T cells that initiates prior to the induction of neutralizing antibodies. Further elucidation of the complexity and function of RV-specific $CD4^+$ T cells, and their relationship to clinical and immune outcomes following infection is warranted.

In summary, we have identified conserved $CD4^+$ T-cell epitopes of rhinovirus capsid proteins that cluster into HLA binding “hotspots.” These peptides, which span narrow molecular regions, will not only provide a valuable tool for evaluating T-cell responses to RV in humans, but could also inform the design of peptide vaccines designed to boost T-cell immunity to multiple RV strains.

Supplementary Material

Refer to Web version on PubMed Central for supplementary material.

Acknowledgments

The authors thank: Ronald Turner, MD (University of Virginia) for his helpful comments; Joanne Lannigan, MS, and Michael Solga, MS (University of Virginia) for assistance with flow cytometry; and Deborah Murphy, RN, and Holliday Carper, BS (University of Virginia) for coordinating RV challenge studies and assisting with blood draws.

Funding Sources: This work was supported by NIH/NIAID U01 AI100799 (J.A.W.) and NIH T32 AI007496 (L.M.M.).

Abbreviations

TGEM	Tetramer-guided epitope mapping
RV	Rhinovirus
pMHCII	Peptide/MHCII
IEDB	Immune Epitope Database
Tfh	T follicular helper

References

1. Louie JK, Yagi S, Nelson FA, Kiang D, Glaser CA, Rosenberg J, Cahill CK, Schnurr DP. Rhinovirus outbreak in a long term care facility for elderly persons associated with unusually high mortality. Clin Infect Dis. 2005; 41:262–5. [PubMed: 15983926]
2. Calhoun WJ, Dick EC, Schwartz LB, Busse WW. A common cold virus, rhinovirus 16, potentiates airway inflammation after segmental antigen bronchoprovocation in allergic subjects. J Clin Invest. 1994; 94:2200–8. [PubMed: 7989575]

3. Gern JE, Calhoun W, Swenson C, Shen G, Busse WW. Rhinovirus infection preferentially increases lower airway responsiveness in allergic subjects. Am J Respir Crit Care Med. 1997; 155:1872–6. [PubMed: 9196088]

4. Heymann PW, Kennedy JL. Rhinovirus-induced asthma exacerbations during childhood: the importance of understanding the atopic status of the host. J Allergy Clin Immunol. 2012; 130:1315–6. [PubMed: 23195527]

5. Cox DW, Bizzintino J, Ferrari G, Khoo SK, Zhang G, Whelan S, Lee WM, Bochkov YA, Geelhoed GC, Goldblatt J, Gern JE, Laing IA, Le Souëf PN. HRV-C Infection in Young Children with Acute Wheeze is Associated with Increased Acute Respiratory Hospital Admissions. Am J Respir Crit Care Med. 2013; 188:1358–64. [PubMed: 23992536]

6. Iwane MK, Prill MM, Lu X, Miller EK, Edwards KM, Hall CB, Griffin MR, Staat MA, Anderson LJ, Williams JV, Weinberg Ga, Ali A, Szilagyi PG, Zhu Y, Erdman DD. Human Rhinovirus Species Associated With Hospitalizations for Acute Respiratory Illness in Young US Children. J Infect Dis. 2011; 204:1702–10. [PubMed: 22013207]

7. Lemanske RF, Jackson DJ, Gangnon RE, Evans MD, Li Z, Shult PA, Kirk CJ, Reisdorf E, Roberg KA, Anderson EL, Carlson-Dakes KT, Adler KJ, Gilbertson-White S, Pappas TE, Dasilva DF, Tisler CJ, Gern JE. Rhinovirus illnesses during infancy predict subsequent childhood wheezing. J Allergy Clin Immunol. 2005; 116:571–577. [PubMed: 16159626]

8. O'Callaghan-Gordo C, Bassat Q, Díez-Padrisa N, Morais L, Machevo S, Nhampossa T, Quintó L, Alonso PL, Roca A. Lower Respiratory Tract Infections Associated with Rhinovirus during Infancy and Increased Risk of Wheezing during Childhood. A Cohort Study. PLoS One. 2013; 8:e69370. [PubMed: 23935997]

9. 2010. Asthma's Impact on the Nation: Data from the CDC National Asthma Control Program

10. Heikkinen T, Järvinen A. The common cold. Lancet. 2003; 361:51–59. [PubMed: 12517470]

11. Nicholson KG, Kent J, Hammersley V, Cancio E. Acute viral infections of upper respiratory tract in elderly people living in the community: comparative, prospective, population based study of disease burden. BMJ. 1997; 315:1060–1064. [PubMed: 9366736]

12. Alper CM, Doyle WJ, Skoner DP, Buchman CA, Seroky JT, Gwaltney JM, Cohen SA. Prechallenge antibodies: moderators of infection rate, signs, and symptoms in adults experimentally challenged with rhinovirus type 39. Laryngoscope. 1996; 106:1298–1305. [PubMed: 8849805]

13. Alper CM, Doyle WJ, Skoner DP, Buchman CA, Cohen S, Gwaltney JM. Prechallenge Antibodies Moderate Disease Expression in Adults Experimentally Exposed to Rhinovirus Strain Hanks. Clin Infect Dis. 1998; 27:119–128. [PubMed: 9675465]

14. Cate TR, Rossen RD, Douglas RG Jr, Butler WT, Couch RB. The role of nasal secretion and serum antibody in the rhinovirus common cold. Am J Epidemiol. 1966; 84:352–363. [PubMed: 4288191]

15. Cate TR, Couch RB, Johnson KM. Studies With Rhinoviruses in Volunteers: Production of Illness, Effect of Naturallly Acquired Antibody, and Demonstration of a Protective Effect Not Associated With Serum Antibody. J Clin Invest. 1964; 43:56–67. [PubMed: 14105232]

16. Barclay WS, Al-Nakib W, Higgins PG, Tyrrell DA. The time course of the humoral immune response to rhinovirus infection. Epidemiol Infect. 1989; 103:659–669. [PubMed: 2558033]

17. Conant RM, Vincent ND. Rhinoviruses: Basis for a numbering system I. HeLa cells for propagation and serologic procedures. J Immunol. 1968; 100:107–113. [PubMed: 4295059]

18. Palmenberg AC, Spiro D, Kuzmickas R, Wang S, Djikeng A, Rathe JA, Fraser-Liggett CM, Liggett SB. Sequencing and analyses of all known human rhinovirus genomes reveal structure and evolution. Science. 2009; 324:55–59. [PubMed: 19213880]

19. Hogan RJ, Zhong W, Usherwood EJ, Cookenham T, Roberts AD, Woodland DL. Protection from respiratory virus infections can be mediated by antigen-specific CD4+ T cells that persist in the lungs. J Exp Med. 2001; 193:981–986. [PubMed: 11304559]

20. Ge X, Tan V, Bollyky PL, Standifer NE, James EA, Kwok WW. Assessment of seasonal influenza A virus-specific CD4 T-cell responses to 2009 pandemic H1N1 swine-origin influenza A virus. J Virol. 2010; 84:3312–9. [PubMed: 20071564]

21. Wilkinson TM, Li CKF, Chui CSC, Huang AKY, Perkins M, Liebner JC, Lambkin-Williams R, Gilbert A, Oxford J, Nicholas B, Staples KJ, Dong T, Douek DC, McMichael AJ, Xu XN.

Preexisting influenza-specific CD4+ T cells correlate with disease protection against influenza challenge in humans. Nat Med. 2012; 18:274–80. [PubMed: 22286307]

22. Parry DE, Busse WW, Sukow KA, Dick CR, Swenson C, Gern JE. Rhinovirus-induced PBMC responses and outcome of experimental infection in allergic subjects. J Allergy Clin Immunol. 2000; 105:692–698. [PubMed: 10756217]
23. Colonno RJ, Condra JH, Mizutani S, Callahan PL, Davies ME, Murcko MA. Evidence for the direct involvement of the rhinovirus canyon in receptor binding. Proc Natl Acad Sci USA. 1988; 85:5449–5453. [PubMed: 2840661]
24. Olson NH, Kolatkar PR, Oliveira Ma, Cheng RH, Greve JM, McClelland A, Baker TS, Rossmann MG. Structure of a human rhinovirus complexed with its receptor molecule. Proc Natl Acad Sci USA. 1993; 90:507–11. [PubMed: 8093643]
25. Bella J, Rossmann MG. ICAM-1 receptors and cold viruses. Pharm Acta Helv. 2000; 74:291–297. [PubMed: 10812972]
26. Bochkov YA, Watters K, Ashraf S, Griggs TF, Devries MK, Jackson DJ, Palmenberg AC, Gern JE. Cadherin-related family member 3, a childhood asthma susceptibility gene product, mediates rhinovirus C binding and replication. Proc Natl Acad Sci. 2015; 112:5485–5490. [PubMed: 25848009]
27. Iwasaki J, Smith WA, Khoo SK, Bizzintino J, Zhang G, Cox DW, Laing IA, Le Souëf PN, Thomas WR, Hales BJ. Comparison of rhinovirus antibody titers in children with asthma exacerbations and species-specific rhinovirus infection. J Allergy Clin Immunol. 2014; 134:25–32. [PubMed: 24767874]
28. McLean GR, Walton RP, Shetty S, Peel TJ, Paktiawal N, Kebadze T, Gogsadze L, Niespodziana K, Valenta R, Bartlett NW, Johnston SL. Rhinovirus infections and immunisation induce cross-serotype reactive antibodies to VP1. Antiviral Res. 2012; 95:193–201. [PubMed: 22742898]
29. Niespodziana K, Cabauatan CR, Jackson DJ, Gallerano D, Trujillo-Torralbo B, del Rosario A, Mallia P, Valenta R, Johnston SL. Rhinovirus-induced VP1-specific Antibodies are Group-specific and Associated With Severity of Respiratory Symptoms. EBioMedicine. 2015; 2:64–70. [PubMed: 26137535]
30. Iwasaki J, Smith WA, Stone SR, Thomas WR, Hales BJ. Species-specific and cross-reactive IgG1 antibody binding to viral capsid protein 1 (VP1) antigens of human rhinovirus species A, B and C. PLoS One. 2013; 8:e70552. [PubMed: 23950960]
31. Glanville N, McLean GR, Guy B, Lecouturier V, Berry C, Girerd Y, Gregoire C, Walton RP, Pearson RM, Kebadze T, Burdin N, Bartlett NW, Almond JW, Johnston SL. Cross-serotype immunity induced by immunization with a conserved rhinovirus capsid protein. PLOS Pathog. 2013; 9:e1003669. [PubMed: 24086140]
32. Kennedy JL, Shaker M, McMeen V, Gern J, Carper H, Murphy D, Lee WM, Bochkov YA, Vrtis RF, Platts-Mills T, Patrie J, Borish L, Steinke JW, Woods WA, Heymann PW. Comparison of Viral Load in Individuals with and without Asthma during Infections with Rhinovirus. Am J Respir Crit Care Med. 2014; 189:532–539. [PubMed: 24471509]
33. Hewson CA, Haas JJ, Bartlett NW, Message SD, Laza-Stanca V, Kebadze T, Caramori G, Zhue J, Edbrooke MR, Stanciu LA, Kon OM, Papi A, Jefferye PK, Edwards MR, Johnston SL. Rhinovirus induces MUC5AC in a human infection model and in vitro via NF-KB and EGFR pathways. Eur Respir J. 2010; 36:1425–1435. [PubMed: 20525715]
34. Grünberg K, Smits HH, Timmers MC, de Klerk EP, Dolhain RJ, Dick EC, Hiemstra PS, Sterk PJ. Experimental rhinovirus 16 infection. Effects on cell differentials and soluble markers in sputum in asthmatic subjects. Am J Respir Crit Care Med. 1997; 156:609–16. [PubMed: 9279247]
35. Bizzintino J, Lee WM, Laing IA, Vang F, Pappas T, Zhang G, Martin AC, Khoo SK, Cox DW, Geelhoed GC, McMinne PC, Goldblatt J, Gern JE, Le Souëf PN. Association between human rhinovirus C and severity of acute asthma in children. Eur Respir J. 2011; 37:1037–1042. [PubMed: 20693244]
36. Calvén J, Yudina Y, Hallgren O, Westergren-Thorsson G, Davies DE, Brandelius A, Uller L. Viral stimuli trigger exaggerated thymic stromal lymphopoietin expression by chronic obstructive pulmonary disease epithelium: role of endosomal TLR3 and cytosolic RIG-I-like helicases. J Innate Immun. 2012; 4:86–99. [PubMed: 21691053]

37. Liu K, Gualano RC, Hibbs ML, Anderson GP, Bozinovski S. Epidermal growth factor receptor signaling to Erk1/2 and STATs control the intensity of the epithelial inflammatory responses to rhinovirus infection. J Biol Chem. 2008; 283:9977–9985. [PubMed: 18276593]
38. Zambrano JC, Carper HT, Rakes GP, Patrie JT, Murphy DD, Platts-Mills TAE, Hayden FG, Gwaltney JM, Hatley TK, Owens AM, Heymann PW. Experimental rhinovirus challenges in adults with mild asthma: Response to infection in relation to IgE. J Allergy Clin Immunol. 2003; 111:1008–1016. [PubMed: 12743565]
39. Turner RB, Weingand KW, Yeh CH, Leedy DW. Association between interleukin-8 concentration in nasal secretions and severity of symptoms of experimental rhinovirus colds. Clin Infect Dis. 1998; 26:840–846. [PubMed: 9564459]
40. Jackson GG, Dowling HF. Transmission of the common cold to volunteers under controlled conditions. IV. Specific immunity to the common cold. J Clin Invest. 1959; 38:762–976. [PubMed: 13654511]
41. Reefer AJ, Carneiro RM, Custis NJ, Platts-Mills TAE, Sung SSJ, Hammer J, Woodfolk JA. A role for IL-10-mediated HLA-DR7-restricted T cell-dependent events in development of the modified Th2 response to cat allergen. J Immunol. 2004; 172:2763–2772. [PubMed: 14978075]
42. Reijonen H, Kwok WW. Use of HLA class II tetramers in tracking antigen-specific T cells and mapping T-cell epitopes. Methods. 2003; 29:282–288. [PubMed: 12725793]
43. The Uniprot Consortium. Activities at the Universal Protein Resource (UniProt). Nucleic Acids Res. 2014; 42:D191–D198. [PubMed: 24253303]
44. Novak EJ, Liu AW, Gebe JA, Falk BA, Nepom GT, Koelle DM, Kwok WW. Tetramer-guided epitope mapping: Rapid identification and characterization of immunodominant CD4+ T cell epitopes from complex antigens. J Immunol. 2001; 166:6665–6670. [PubMed: 11359821]
45. Kwok WW, Roti M, DeLong JH, Tan V, Wambre E, James EA, Robinson D. Direct ex vivo analysis of allergen-specific CD4+ T cells. J Allergy Clin Immunol. 2010; 125:1407–1409. [PubMed: 20513526]
46. Danke NA, Koelle DM, Yee C, Beheray S, Kwok WW. Autoreactive T cells in healthy individuals. J Immunol. 2004; 172:5967–72. [PubMed: 15128778]
47. Hulse KE, Reefer AJ, Engelhard VH, Patrie JT, Ziegler SF, Chapman MD, Woodfolk JA. Targeting Allergen to FcgammaRI Reveals a Novel Th2 Regulatory Pathway Linked to TSLP Receptor. J Allergy Clin Immunol. 2010; 125:247–264. [PubMed: 20109752]
48. Roederer M, Nozzi JL, Nason MC. SPICE: exploration and analysis of post-cytometric complex multivariate datasets. Cytometry A. 2011; 79:167–74. [PubMed: 21265010]
49. Altschul SF, Gish W, Miller W, Myers EW, Lipman DJ. Basic Local Alignment Search Tool. J Mol Biol. 1990; 215:403–410. [PubMed: 2231712]
50. Waterhouse AM, Procter JB, Martin DMA, Clamp M, Barton GJ. Jalview Version 2- a multiple sequence alignment editor and analysis workbench. Bioinformatics. 2009; 25:1189–1191. [PubMed: 19151095]
51. Wang P, Sidney J, Kim Y, Sette A, Lund O, Nielsen M, Peters B. Peptide binding predictions for HLA DR, DP and DQ molecules. BMC Bioinformatics. 2010; 11:568. [PubMed: 21092157]
52. Wang P, Sidney J, Dow C, Mothé B, Sette A, Peters B. A systematic assessment of MHC class II peptide binding predictions and evaluation of a consensus approach. PLOS Comput Biol. 2008; 4:e1000048. [PubMed: 18389056]
53. Nielsen M, Lundegaard C, Lund O. Prediction of MHC class II binding affinity using SMM-align, a novel stabilization matrix alignment method. BMC Bioinformatics. 2007; 8:238. [PubMed: 17608956]
54. Nielsen M, Lund O. NN-align. An artificial neural network-based alignment algorithm for MHC class II peptide binding prediction. BMC Bioinformatics. 2009; 10:296. [PubMed: 19765293]
55. Sturniolo T, Bono E, Ding J, Raddrizzani L, Tuereci O, Sahin U, Braxenthaler M, Gallazzi F, Protti MP, Sinigaglia F, Hammer J. Generation of tissue-specific and promiscuous HLA ligand databases using DNA microarrays and virtual HLA class II matrices. Nat Biotechnol. 1999; 17:555–561. [PubMed: 10385319]

56. Zhang GL, DeLuca DS, Keskin DB, Chitkushev L, Zlateva T, Lund O, Reinherz EL, Brusic V. MULTIPRED2: a computational system for large-scale identification of peptides predicted to bind to HLA supertypes and alleles. J Immunol Methods. 2011; 374:53–61. [PubMed: 21130094]
57. Karosiene E, Rasmussen M, Blicher T, Lund O, Buus S, Nielsen M. NetMHCIIpan-3.0, a common pan-specific MHC class II prediction method including all three human MHC class II isotypes, HLA-DR, HLA-DP and HLA-DQ. Immunogenetics. 2013; 65:711–724. [PubMed: 23900783]
58. Nielsen M, Lundegaard C, Blicher T, Lamberth K, Harndahl M, Justesen S, Røder G, Peters B, Sette A, Lund O, Buus S. NetMHCpan, a method for quantitative predictions of peptide binding to any HLA-A and -B locus protein of known sequence. PLoS One. 2007; 2:e796. [PubMed: 17726526]
59. Hoof I, Peters B, Sidney J, Pedersen LE, Sette A, Lund O, Buus S, Nielsen M. NetMHCpan, a method for MHC class I binding prediction beyond humans. Immunogenetics. 2009; 61:1–13. [PubMed: 19002680]
60. DeLano W. The PyMOL Molecular Graphics System. 2002
61. Hadfield AT, Lee WM, Zhao R, Oliveira MA, Minor I, Rueckert RR, Rossmann MG. The refined structure of human rhinovirus 16 at 2.15 A resolution: Implications for the viral life cycle. Structure. 1997; 5:427–441. [PubMed: 9083115]
62. Agrawal R, Wisniewski J, Yu MD, Kennedy JL, Platts-Mills T, Heymann PW, Woodfolk JA. Infection with human rhinovirus 16 promotes enhanced IgE responsiveness in basophils of atopic asthmatics. Clin Exp Allergy. 2014; 44:1266–1273. [PubMed: 25113532]
63. McIntyre CL, Knowles NJ, Simmonds P. Proposals for the classification of human rhinovirus species A, B and C into genotypically assigned types. J Gen Virol. 2013; 94:1791–1806. [PubMed: 23677786]
64. Oliveira M, Zhao R, Lee W, Kremer M. The structure of human rhinovirus 16. Structure. 1993; 1:51–68. [PubMed: 7915182]
65. Yamamoto J, Adachi Y, Onoue Y, Adachi YS, Okabe Y, Itazawa T, Toyoda M, Seki T, Morohashi M, Matsushima K. Differential expression of the chemokine receptors by the Th1- and Th2-type effector populations within circulating CD4+ T cells. J Leukoc Biol. 2000; 68:568–574. [PubMed: 11037980]
66. Groom JR, Luster AD. CXCR3 in T Cell Function. Exp Cell Res. 2011; 317:620–631. [PubMed: 21376175]
67. van Oosterwijk MF, Juwana H, Arens R, Tesselaar K, van Oers MHJ, Eldering E, van Lier RAW. CD27-CD70 interactions sensitise naive CD4+ T cells for IL-12-induced Th1 cell development. Int Immunol. 2007; 19:713–8. [PubMed: 17548342]
68. Mahon BP, Katrak K, Nomoto A, Macadam AJ, Minor PD, Mills KHG. Poliovirus-Specific CD4+ Th1 Clones with Both Cytotoxic and Helper Activity Mediate Protective Humoral Immunity against a Lethal Poliovirus Infection in Transgenic Mice Expressing the Human Poliovirus Receptor. J Exp Med. 1995; 181:1285–1292. [PubMed: 7699320]
69. Morita R, Schmitt N, Bentebibel SE, Ranganathan R, Bourdery L, Zurawski G, Foucat E, Dullaers M, Oh S, Sabzghabaei N, Lavecchio EM, Punaro M, Pascual V, Banchereau J, Ueno H. Human blood CXCR5+CD4+ T cells are counterparts of T follicular cells and contain specific subsets that differentially support antibody secretion. Immunity. 2011; 34:108–21. [PubMed: 21215658]
70. Crotty S. Follicular helper CD4 T cells (Tfh). Annu Rev Immunol. 2011; 29:621–63. [PubMed: 21314428]
71. Yang J, James EA, Sanda S, Greenbaum C, Kwok WW. CD4+ T cells recognize diverse epitopes within GAD65: implications for repertoire development and diabetes monitoring. Immunology. 2013; 138:269–79. [PubMed: 23228173]
72. James EA, LaFond RE, Gates TJ, Mai DT, Malhotra U, Kwok WW. Yellow fever vaccination elicits broad functional CD4+ T cell responses that recognize structural and nonstructural proteins. J Virol. 2013; 87:12794–804. [PubMed: 24049183]
73. James EA, Bui J, Berger D, Huston L, Roti M, Kwok WW. Tetramer-guided epitope mapping reveals broad, individualized repertoires of tetanus toxin-specific CD4+ T cells and suggests HLA-based differences in epitope recognition. Int Immunol. 2007; 19:1291–1301. [PubMed: 17906339]

74. Yang J, James EA, Huston L, Danke NA, Liu AW, Kwok WW. Multiplex mapping of CD4 T cell epitopes using class II tetramers. Clin Immunol. 2006; 120:21–32. [PubMed: 16677863]

75. Woodfolk JA, Sung SS, Benjamin DC, Lee JK, Platts-Mills TAE. Distinct human T cell repertoires mediate immediate and delayed-type hypersensitivity to the Trichophyton antigen, Tri r 2. J Immunol. 2000; 165:4379–4387. [PubMed: 11035075]

76. Su LF, Kidd BA, Han A, Kotzin JJ, Davis MM. Virus-specific CD4+ memory-phenotype T cells are abundant in unexposed adults. Immunity. 2013; 38:373–83. [PubMed: 23395677]

77. Kistler AL, Webster DR, Rouskin S, Magrini V, Credle JJ, Schnurr DP, Boushey HA, Mardis ER, Li H, DeRisi JL. Genome-wide diversity and selective pressure in the human rhinovirus. Virol J. 2007; 4:40. [PubMed: 17477878]

78. Panjwani A, Strauss M, Gold S, Wenham H, Jackson T, Chou JJ, Rowlands DJ, Stonehouse NJ, Hogle JM, Tuthill TJ. Capsid Protein VP4 of Human Rhinovirus Induces Membrane Permeability by the Formation of a Size-Selective Multimeric Pore. PLoS Pathog. 2014; 10:1–12.

79. Gern JE, Dick EC, Kelly EA, Vrtis R, Klein B. Rhinovirus-specific T cells recognize both shared and serotype-restricted viral epitopes. J Infect Dis. 1997; 175:1108–1114. [PubMed: 9129073]

80. Hastings GZ, Rowlands DJ, Francis MJ. Proliferative responses of T cells primed against human rhinovirus to other rhinovirus serotypes. J Gen Virol. 1991; 72:2947–2952. [PubMed: 1722503]

81. Hadfield AT, Oliveira MA, Kim KH, Minor I, Kremer MJ, Heinz BA, Shepard D, Pevear DC, Rueckert RR, Rossmann MG. Structural studies on human rhinovirus 14 drug-resistant compensation mutants. J Mol Biol. 1995; 253:61–73. [PubMed: 7473717]

A

HLA Allele	Epitope	Amino Acid Position	Consensus Rank	NetMHCIIpan 9mer IC_{50}	NetMHCIIpan 19mer IC_{50}
1*0101	$VP1_{P23}$ PRFSLPFLSIASAYYMFYDG	181-200	***1.58***	***172.97***	***5.67***
	$VP2_{P24}$ PHQFINLRSNNSATLIVPYV	186-205	***3***	***181.55***	***8.98***
1*0301	$VP2_{P21}$ NEKQPSDDNWLNFDGTLLGN	162-181	***1.03***	4370.08	***302.6***
1*0401	$VP2_{P21}$ NEKQPSDDNWLNFDGTLLGN	162-181	***3.81***	5426.27	549.54
1*0404	$VP1_{P18}$ HIVMQYMYVPPGAPIPTTRD	141-160	***0.17***	6965.00	***151.24***
	$VP2_{P3}$ RGDSTITSQDVANAVVGYGV	18-37	12.10	10711.98	***459.38***
1*0701	$VP1_{P23}$ PRFSLPFLSIASAYYMFYDG	181-200	***1.41***	***475.46***	***14.74***
	$VP2_{P26}$ VPYVNAVPMDSMVRHNNWSL	202-221	***3.75***	6153.57	***287.34***
1*1101	$VP2_{P2}$ SDRIIQITRGDSTITSQDVA	10-29	***1.33***	3995.77	696.30
1*1501	$VP2_{P25}$ SNNSATLIVPYVNAVPMDSM	194-213	***6.64***	9592.89	***298.16***
DRB5	$VP1_{P21}$ QSGTNASVFWQHGQPFPRFS	165-184	***1.02***	2664.32	***38.55***
	$VP2_{P10}$ TSKGWWWKLPDALKDMGIFG	74-93	***2.85***	1218.18	***91.2***

B

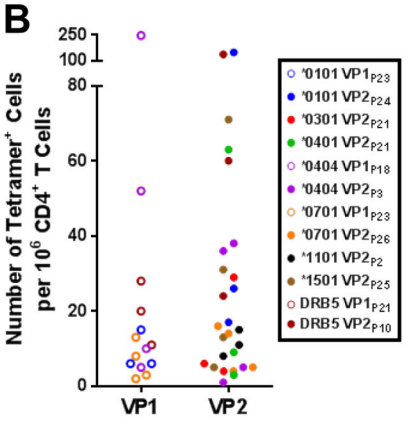

C

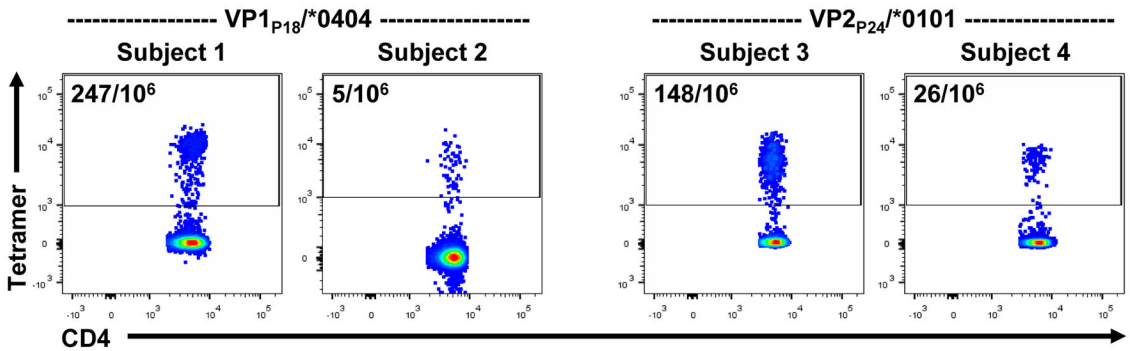

D

Fig. 1. VP1 and VP2 Epitopes of RV-A16

(A) Epitopes identified by TGEM (VP1 epitopes shaded) and their predicted binding constants. Underline denotes predicted 9mer core epitope. Consensus rank was generated using the IEDB resource. The NetMHCIIpan algorithm was used to compare predictions for 9mer and 19mer epitopes. Bolded values meet defined criteria for MHCII binding (IEDB Consensus Rank ≤10; NetMHCIIpan IC_{50} ≤500). **(B)** Frequencies of RV-specific $CD4^+$ T cells determined by direct *ex vivo* staining with tetramer for each TGEM epitope (29 subjects). **(C)** Representative data showing $tetramer^+$ T cells within the $CD4^+$ T-cell gate stained with $VP1_{P18}$/*0404 and $VP2_{P24}$/*0101 tetramers in 4 subjects with high and low T-

cell frequencies. **(D)** Localization of T-cell epitopes within the primary amino acid sequences of VP1 and VP2. Line denotes each 20mer peptide with predicted core epitopes in grey.

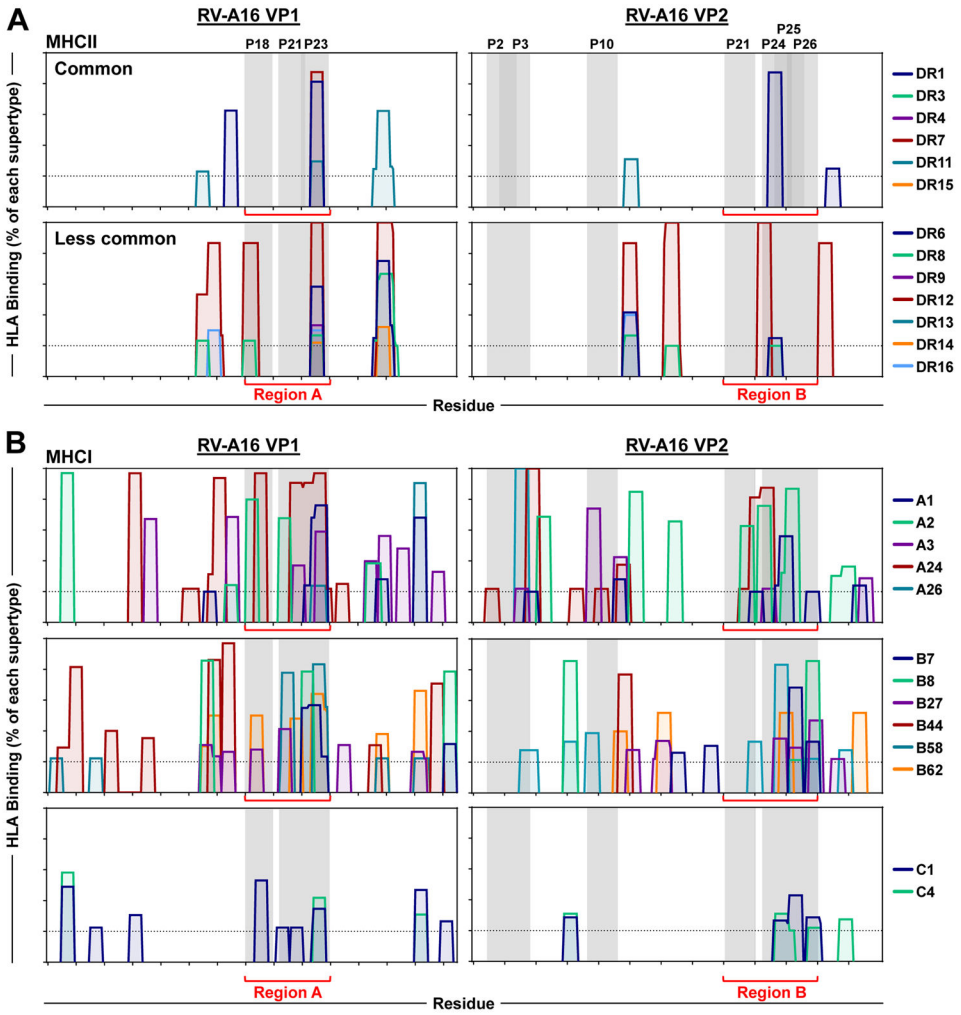

Fig 2. HLA Class I and II Binding "Hotspots" Localize to Conserved Regions of VP1 and VP2

Epitope binding to HLA class I and II supertypes was analyzed for RV-A16 VP1 and VP2 using MULTIPRED2. The percentage binding is shown for each supertype corresponding to: **(A)** common class II DRB1 supertypes that include molecules used in TGEM studies, as well as less common class II DRB1 supertypes; and **(B)** the major class I supertypes, HLA-A, -B, and -C. Analysis of DRB5 supertypes was not available. Data was generated using an IC_{50} threshold of ≤500 nM. Epitopes with predicted binding to ≥20% of molecules corresponding to each HLA supertype are shown.

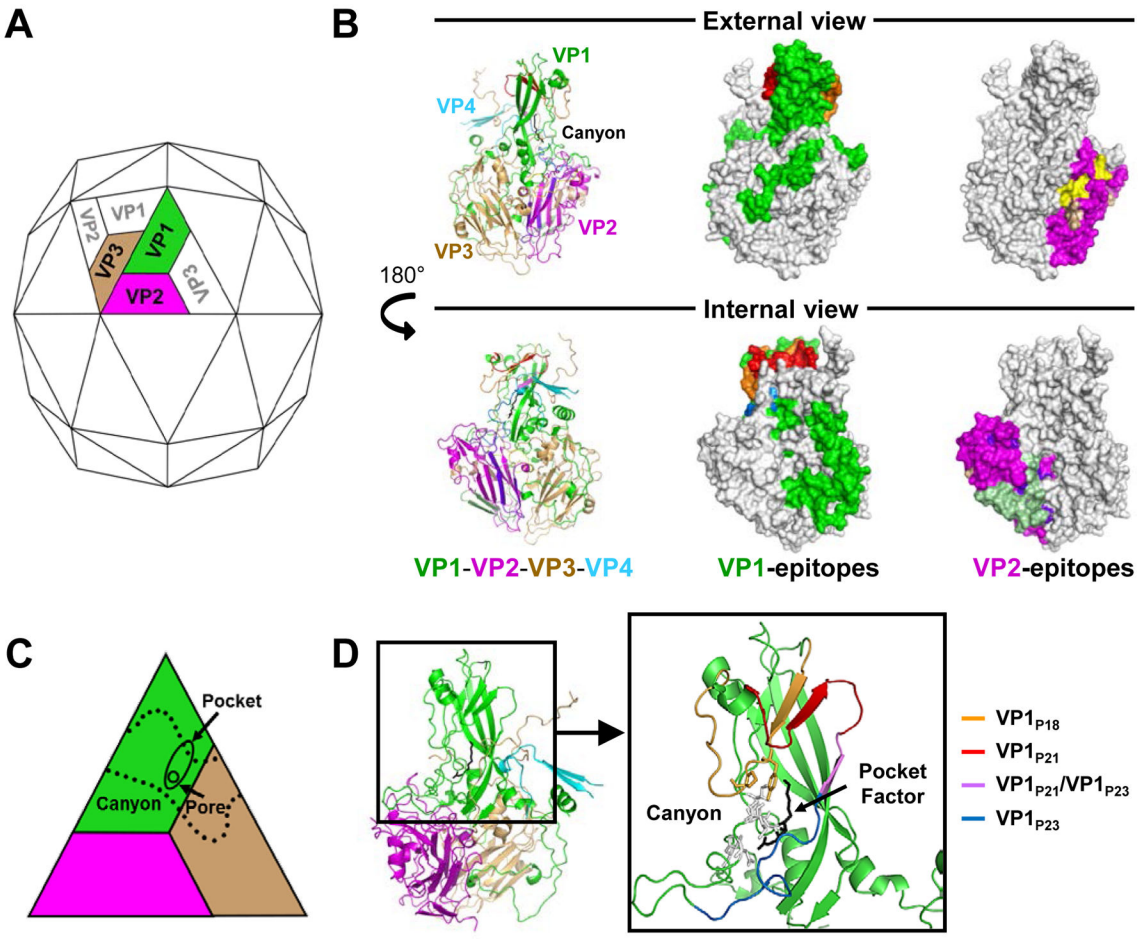

Fig. 3. Position of CD4$^+$ T-Cell Epitopes of RV-A16 Within the Capsid Structure

(A) Model showing the position of the oligomeric subunit on the external aspect of the capsid. VP1, VP2 and VP3 are visible, while VP4 resides on the internal aspect. **(B)** External and internal views of T-cell epitopes within the oligomeric subunit (VP1-4). T-cell epitopes are colored as follows: VP1: P18 (orange), P21 (red), P23 (blue) with the 4 overlapping residues between P21 and P23 in violet (overlap hidden from the surface, visible in D); and VP2: P2 and P3 (light green), P10 (wheat), P21 (yellow) and P24-P25-P26 (dark blue). **(C)** Footprint of the canyon in relation to the triangular capsid subunit formed by VP1+VP2 from one subunit, and VP3 from the adjacent subunit. The drug binding pocket extends from a pore at the base of the canyon into a larger cavity within the core of VP1. Schematic adapted from (81). **(D)** Localization of the canyon and the pocket binding factor in VP1 in relation to VP2 and VP3, viewed from the inside of the capsid. Expanded view depicts VP1 only for simplicity, with the T-cell epitopes in color as described in B. Residues which have an atom lying within 4 angstroms of the pocket factor are shown as white sticks and include Ile1098, Asn1099, Leu1100, Asn1212, Met1214, and His 1260 (61). Two residues of $VP1_{P18}$ associated with the binding pocket (Tyr 1144 and Pro1146) are shown in orange. Lauric acid, a representative pocket factor, is shown as a black stick model in the ribbon models in B and D.

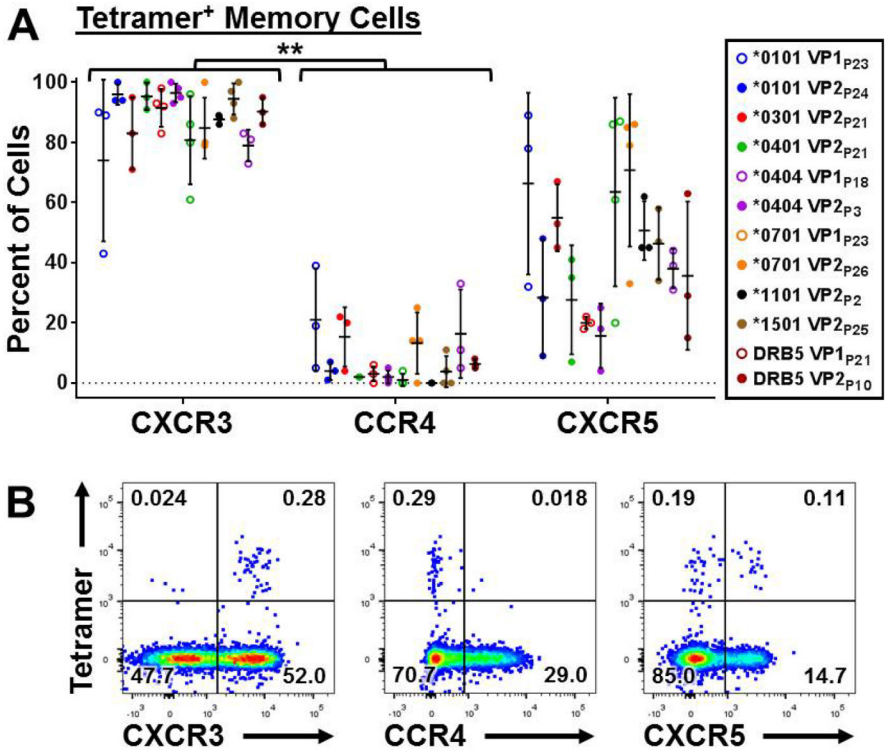

Fig 4. Pre-existing Epitope-Specific Memory Cells Display Th1 and Tfh Signatures

(A) Surface phenotype of tetramer^{+} memory (CD45RA^{neg}) CD4^{+} T cells analyzed directly *ex vivo* in 29 healthy subjects with diverse HLA types (3–4 subjects per tetramer). Bars denote the mean ±SD. **(B)** Representative data from one subject showing expression of surface markers on memory CD4^{+} T cells. **p<0.0001.

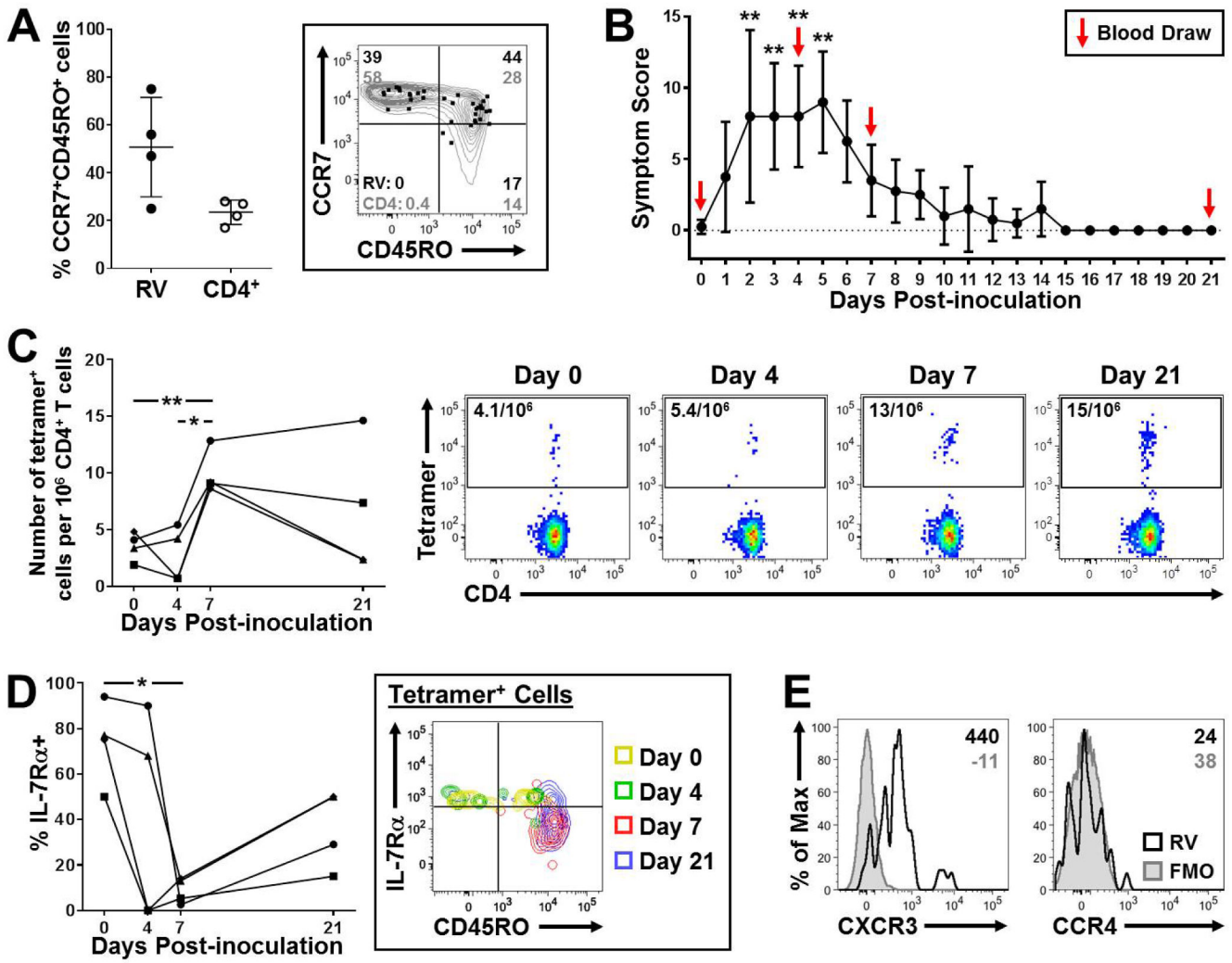

Fig 5. Pre-existing Epitope-Specific Th1 Cells Expand and are Activated *In Vivo* Following Experimental Infection with RV-A16

(A–F) Four seronegative subjects (three *0401+ and one *0301+) were inoculated intranasally with RV-A16. Tetramer staining was performed immediately prior to inoculation (day 0), and at days 4, 7 and 21 post-inoculation using $VP2_{P21}$/*0401 or $VP2_{P21}$/*0301 tetramers. **(A)** Analysis of $CCR7^+CD45RO^+$ cells within tetramer$^+$ and total $CD4^+$ T cells at day 0. Panel on right shows representative data from one subject for RV-specific (dot) and total $CD4^+$ (contour) T cells. **(B)** Upper respiratory tract symptom scores at days 0–21 (mean ± SD). **(C)** Change in numbers of tetramer$^+$ T cells during infection. Scatter plots show representative data gated on total $CD4^+$ T cells. **(D)** Change in expression of IL-7Rα on tetramer$^+$ cells during infection. Panel on right shows representative data for IL-7Rα against CD45RO on tetramer$^+$ cells. **(E)** Representative data showing the expression of CXCR3 and CCR4 on tetramer$^+$ cells at 7 days post-inoculation. Values denote median fluorescence intensity. *p<0.05, **p<0.01.

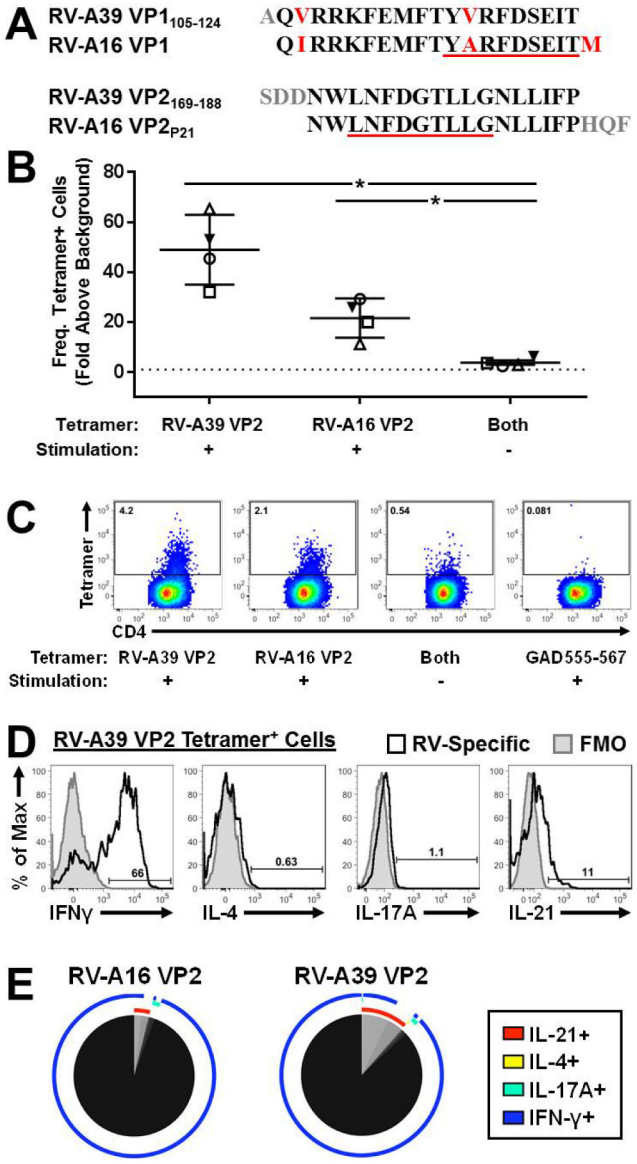

Fig 6. Proof-of-Concept of T-Cell Cross-Reactivity at the Epitope Level

(A) Alignment of two *0401-restricted epitopes of RV-A39 with corresponding RV-A16 sequences. Predicted core epitopes are underlined, and altered residues are shown in red. Grey residues denote different flanking residues. **(B)** Cells from four *0401+ seronegative subjects were either stimulated with RV-A39 $VP2_{169-188}$ (+) or unstimulated (−) for 14 days. Cells were then stained with *0401 tetramers displaying RV-A39 $VP2_{169-188}$ or RV-A16 $VP2_{P21.}$ Stimulated cells stained with tetramers displaying an irrelevant peptide (GAD555-567) provided a negative control. Frequencies of $tetramer^+$ T cells are shown relative to numbers obtained using *0401/GAD555-567 tetramer. Bars denote the mean ± SD. *$p<0.05$. **(C)** Scatter plots showing representative tetramer staining. **(D)** Representative histograms showing cytokine expression in RV-A39 VP2 $tetramer^+$ T cells after culture. **(E)** Average cytokine profiles for RV-A16 and RV-A39 VP2-specific $CD4^+$ T cells after

stimulation with RV-A39 $VP2_{169\text{-}188}$ analyzed by SPICE (4 subjects). Each pie slice denotes a discrete T-cell phenotype, and colored arcs denote each cytokine in relation to each phenotype.

Table I

Sequence Similarity Between RV-A16 Epitopes and Rhinovirus Strains Belonging to Species A, B, and C.

	Prevalence of Amino Acid Sequence Identity Among Strains of Each Rhinovirus Species								
	RV A					RV B		RV C	
Epitope	100%	99–95%	94–90%	89–85%	Total	Total	Range (% identity)	Total	Range (% identity)
VP2P3 RGDSTITSQDVANAVVGYGV	40/77 (51.9%)	17/77 (22.1%)	10/77 (13.0%)	7/77 (9.1%)	74/77 (96.1%)	10/29 (34.5%)	72–67%	1/51 (2.0%)	72%
VP2P2 SDRIIQITRGDSTITSQDVA	50/77 (64.9%)	8/77 (10.4%)	13/77 (16.9%)	2/77 (2.6%)	73/77 (94.8%)	23/29 (79.3%)	65%	21/51 (41.2%)	78–72%
VP1P23 PRFSLPFLSIASAYYMFYDG	39/77 (50.6%)	14/77 (18.2%)	3/77 (3.9%)	17/77 (22.1%)	73/77 (94.8%)	21/29 (72.4%)	74–68%	7/51 (13.7%)	70–65%
VP2P26 VPYVNAVPMDSMVRHNNWSL	8/77 (10.4%)	53/77 (68.8%)	5/77 (6.5%)	6/77 (7.8%)	72/77 (93.5%)	23/29 (79.3%)	82–71%	7/51 (13.7%)	76–70%
VP2P10 TSKGWWWKLPDALKDMGIFG	31/77 (40.3%)	33/77 (42.9%)	1/77 (1.3%)	7/77 (9.1%)	72/77 (93.5%)	21/29 (72.4%)	95–84%	4/51 (7.8%)	89–79%
VP2P24 PHQFINLRSNNSATLIVPYV	7/77 (9.1%)	43/77 (55.8%)	12/77 (15.6%)	8/77 (10.4%)	70/77 (90.9%)	23/29 (79.3%)	85–70%	7/51 (13.7%)	75–70%
VP2P25 SNNSATLIVPYVNAVPMDSM	7/77 (9.1%)	59/77 (76.6%)	4/77 (5.2%)	0/77 (0.0%)	70/77 (90.9%)	22/29 (75.9%)	84–68%	7/51 (13.7%)	74–68%
VP1P21 QSGTNASVFWQHGQPFPRFS	2/77 (2.6%)	16/77 (20.8%)	21/77 (27.3%)	29/77 (37.7%)	68/77 (88.3%)	0/29 (0.0%)	---	0/51 (0.0%)	---
VP2P21 NEKQPSDDNWLNFDGTLLGN	17/77 (22.1%)	5/77 (6.5%)	20/77 (26.0%)	9/77 (11.7%)	51/77 (66.2%)	6/29 (20.7%)	89%	0/51 (0.0%)	---
VP1P18 HIVMQYMYVPPGAPIPTTRD	1/77 (1.3%)	3/77 (3.9%)	8/77 (10.4%)	28/77 (36.4%)	40/77 (51.9%)	3/29 (10.3%)	79–54%	0/51 (0.0%)	---

Data was generated based on sequence alignments obtained by Protein BLAST using the top 5,000 results. Peptides are listed from highest to lowest “identity scores” based on their overall prevalence of identity within RV species A.

Values denote the prevalence of strains within each RV species that showed amino acid sequence identity, with percentages in parentheses. The total number of RV types for each species used as the denominator is based on classifications according to McIntyre et al (63).

For RV species B and C, only the total prevalence with the corresponding range of amino acid sequence identity is shown, owing to lower sequence identities compared with RV species A.